Dynamical properties of two- and three-dimensional colloidal clusters of six particles

B. Fačkovec and J. W. R. Morgan and D. J. Wales

Department of Chemistry, University of Cambridge, Lensfield Road, CB2 1EW, Cambridge, UK[*]

(Dated: March 8, 2016)

Colloidal clusters are important systems for studying self-assembly. Clusters of six colloidal particles attracting each other via short-ranged interactions have been recently studied both theoretically and experimentally. Here we present a computer modelling study of the thermodynamics and dynamics of clusters using a short-ranged Morse potential in two and three dimensions. We combine energy landscape methods with comprehensive sampling both of configurations using Markov chain Monte Carlo and also of trajectories using Langevin molecular dynamics propagation. We show that the interaction energies between the particles are greater than previously assumed. The rates predicted by transition state theory using harmonic vibrational densities of states are off by four orders of magnitude, since the effects of viscosity are not accounted for. In contrast, sampling short trajectories using an appropriate friction constant and discrete relaxation path sampling produces reasonable agreement with the experimental rates.

I. INTRODUCTION

Recent work on colloidal particles has involved direct observations of the structures of small clusters and transitions between them, both in two and three dimensions.[1–3] Since the experimental transition rates are now available for two-dimensional and three-dimensional clusters of six particles, it is possible to compare various theoretical techniques for estimating these rates. The experiments enable us to make comparisons at an unprecedented level of detail. Hence we can benchmark our predictions of structure, dynamics and thermodynamics, paving the way for future investigations of larger colloidal clusters, which may help to guide experiment.

The Morse potential[4] has previously been used to model colloidal particles.[5–9] The model treats each particle as a single isotropic site[10] and approximates the full interparticle interaction as pairwise additive. Deviations from pairwise additivity are significant when the range of the potential is large compared to the equilibrium interparticle separation.[11] However, the experimental data was obtained under conditions where the effective interaction range is small.

Transition state theory (TST)[12–21] can be applied to a database of minima and transition states. This theory treats each rearrangement in terms of passage over an energy barrier. The colloidal system is heavily damped by the water solvent, and so viscosity plays an important role in the rearrangements and basic TST is unlikely to give an accurate estimate.[3] The Kramers formulation of the transition state method[22,23] includes effects caused by solvent viscosity. However, the Kramers' assumption of a parabolic energy profile is not satisfied for the Morse rearrangements.[5] On the other hand, if the diffusion constants and path lengths are similar for all the rearrangements, then the relative rates may be correct with only a constant correction factor required.

The geometrical approach of Holmes-Cerfon *et al.*[24]

treats the rearrangement in two parts: first a contact breaking phase and second a diffusive phase at constant energy terminated by formation of one or more new contacts. Results from this method appear to agree well with experimental data.[3]

Short-ranged Morse clusters are challenging systems to simulate. The low-energy regions of phase space have the form of narrow channels: while some degrees of freedom are very stiff, the degrees of freedom relevant for structural transitions are so soft that the norm of the gradient in these directions can underflow numerical precision. Since small time steps are required to achieve stable molecular dynamics propagations, sampling of the phase space can be computationally expensive and an enhanced sampling method is desirable. In cases when the potential energy barrier is comparable to the thermal energy, an assumption that most of the population is centred around low-energy structures is unreliable. Hence, methods that require void space to decorrelate trajectories (such as the transmission coefficient approach[25] or transition path sampling (TPS)[26,27]) may not be accurate.

Discrete relaxation path sampling (DRPS)[28] is a recently developed method for studying rare events that combines the advantages of the energy landscapes framework with rigorous sampling of molecular dynamics trajectories. DRPS has been shown to give robust and reliable rate constants for the whole range of friction regimes, from microcanonical ensembles (no friction) to overdamped systems (no momenta). The relaxation approach of DRPS captures long-timescale behaviour unattainable by reactive flux methods (such as hyperdynamics[29] and boxed molecular dynamics[30]). A systematic reduction of the computational cost can be achieved by constraining molecular dynamics simulations to *a priori* defined cells in configurational space. A memory loss approximation at the cell boundaries is employed, similar to that used by milestoning.[31] However, unlike milestoning (which provides surface-to-surface transition times), DRPS directly provides the rate matrix for cell-to-cell transitions. An obvious advantage over Markov state modelling via short molecular dynamics simulations[32,33] is that the embedding problem does not arise.[34]

[*] research@fackovec.net, dw34@cam.ac.uk

In the present work, we simulate the thermodynamics and kinetics of clusters of six Morse particles in both two and three dimensions. The paper is organised as follows. In Sec. II we summarise results of previous experimental work for six particle colloidal clusters and describe the simulation methods used in the present work. The results obtained from TST and DRPS calculations are presented in Sec. III. In both Sec. II and Sec. III, we first consider two-dimensional clusters and then the three-dimensional analogues. Conclusions are presented in Sec. IV.

II. METHODS

A. Experimental setup

The two-dimensional experiment is described in Ref. 3. Polystyrene (PS) spheres with diameter $\sigma_0 = 1.3 \mu$m were strongly bound to a coverslip of a sample cell. The three-dimensional experiment is described in the supporting material to Ref. 1. For the three-dimensional cluster experiments, PS spheres with diameter $\sigma_0 = 1$ μm were placed in a suspension of poly(N'-Isopropylacrylamide) (PNIPAM) spheres with diameter $r_s = 80$ nm dispersed in 15 mM NaCl and 0.1% P123. Sodium dodecyl sulfate (SDS) micelles were used for studies of two-dimensional clusters instead of the PNIPAM spheres.[3] The solution was constrained to a cylindrical container with diameter $d_c = 30$ μm and height $h_c = 30$ μm. The PS spheres attract each other due to depletion, electrostatic and Derjaguin-Landau-Verwey-Overbeek (DLVO)[35,36] interactions. The interaction was estimated by the authors as around $2k_BT$ (k_B being the Boltzmann constant and T the temperature), but they suggest[1] that "The true well depth in our system is probably closer to $4k_BT$, as estimated from the typical time for cluster rearrangements, which is on the order of tens to hundreds of seconds." For reasons explained in Sec. III A 3, we believe the well depth may be between $6\,k_BT$ and $8\,k_BT$.

We also note that in unpublished work we have found that the global minima for a DLVO potential as a function of cluster size are reproduced by the short-ranged Morse form. This representation was therefore employed, since a clear physical interpretation of all the parameters is possible.

B. The potential and simulation parameters in reduced units

The system can be modelled by a Morse potential with range parameter $\rho = 30$ and well depth of a few k_BT. In natural units the well depth is $\epsilon_0 = 1$ and the collision diameter is $\sigma_0 = 1$. The pairwise potential, written as a function of the interparticle distance R, is

$$V = e^{\rho(1-R)}(e^{\rho(1-R)} - 2).$$ (1)

The well depth defining the reduced units was chosen as $7k_BT$ for 2D clusters and $6k_BT$ for 3D clusters.

1. Two-dimensional clusters

To convert from reduced units to experimental units, some properties of the experimental system must be known. Assuming the density of PS $\rho_{PS} \approx 1000$ kg m^{-3}, the mass of a PS sphere in the 2D experiment is about $\mu_0 = 1.15 \times 10^{-15}$ kg. The natural unit of time is $\tau_0 = \sigma_0 \sqrt{\mu_0/\epsilon_0} = 2.59 \times 10^{-4}$ s; all the calculated rate constants have units of τ_0^{-1}.

The friction constant of the environment has to be estimated for MD simulations. The viscosity of the suspension can be evaluated using the formula by Verberg et al.[37]

$$\eta = \eta_0 \left(1 + \frac{5}{2}\phi + 6\phi^2\right) ,$$ (2)

where η_0 is the dynamical viscosity of the solvent and ϕ is the volume fraction of the dispersed colloidal particles. Using the Stokes formula

$$\gamma = 3\pi\eta d_c ,$$ (3)

we obtain $\gamma = 1.23 \times 10^{-8}$ kg s^{-1} (diffusion coefficient $D_{theo} = 3.38 \times 10^{-13}$ m^2 s^{-1}), which is reasonably consistent with the diffusion coefficient $D_{exp} = 3.1 \times 10^{-13}$ m^2 s^{-1} reported in Ref. 2. The friction constant expressed in reduced units is $\gamma \approx 3000\mu_0/\tau_0$, suggesting high damping.

2. Three-dimensional clusters

The particles used in the 3D experiments were somewhat smaller than the ones used for the 2D experiments. Under the same density assumption, the corresponding reduced mass $\mu_0^{3D} = 5.2 \times 10^{-16}$ kg and the reduced time is $\tau_0^{3D} = 1.45 \times 10^{-4}$ s; The friction constant corresponding to the experimental setup was estimated as above, giving $\gamma^{3D} \approx 5000\ \mu_0^{3D}\ /\ \tau_0^{3D}$.

C. Transition state theory calculations

For our calculations, a database of minima and transition states is required. First basin-hopping,[38–41] as implemented in GMIN,[42] was used to locate the putative global potential energy minimum and other low-lying local minima. The doubly-nudged[43,44] elastic band[45–47] algorithm was used to identify candidate transition states (according to the Murrell-Laidler definition[48]) between all pairs of minima, which were then converged using a hybrid eigenvector-following approach.[49] These procedures are implemented in OPTIM.[50] The minima and transition states thus located were used to seed a PATHSAMPLE[51] database.[52,53] Further searches were conducted until the database ceased to grow and so it was likely that all minima and transition states had been found. PATHSAMPLE was further used to calculate the TST rates between pairs of minima using harmonic vibrational densities of states, combined with a graph transformation procedure to generate overall rate constants.[54–57]

D. Sampling thermodynamics

Parallel tempering Metropolis Monte Carlo[58] was performed for the 2D cluster at 14 different reciprocal temperatures $\beta\epsilon_0 \in \{3, 3.5, 4, 4.5, 5, 5.5, 6, 6.5, 6.75, 7, 7.5, 8, 8.5, 9\}$. A cylindrical container with radius $r_{max} = 3\sigma_0$ was used to avoid sampling dissociated structures. About 10^8 simple steps moving randomly selected particles by a normally distributed displacement with standard deviation of $h = 0.01\sigma_0$ were required to reach satisfactory convergence of the equilibrium populations.

The initial 3D structures for MD were obtained from a long molecular dynamics trajectory using a Langevin propagator[59] with friction constant $\gamma^{3D} = 20\mu_0^{3D}/\tau_0^{3D}$ for each β. An independent trajectory of 10^8 steps was initiated from each minimum.

E. DRPS construction of rate matrices

Sampling was enhanced and parallelised by constraining dynamics to 115 cells and propagating each short trajectory independently. The cells correspond to observable topologies of the cluster (see Fig. 1) and also represent milestones on the transition paths, which are referred to as intermediates and assigned automatically. DRPS is used to construct a 115 x 115 matrix of rates between structures defined by the cells.

For each starting structure $\mathbf{x}_i$ obtained from the parallel tempering simulations, velocities $\mathbf{v}_i$ were randomly generated according to the Maxwell-Boltzmann distribution and the structure was propagated using a Langevin propagator[59] with time step $\Delta t = 0.002\tau_0$ until it left the original cell. Then another simulation was initiated from the same structure $\mathbf{x}_i$ with reversed velocity $-\mathbf{v}_i$ to obtain a boundary-to-boundary trajectory in the original cell. The total simulation time per cell at a given friction constant and reciprocal temperature was on average $3 \times 10^4\tau_0$, which sums to about 2×10^9 gradient calculations for the rate matrix construction at a specific reciprocal temperature and friction constant.

The rate matrices were constructed using the analytical approach suggested in Ref. 28. For each pair of cells that had trajectories exiting to a common boundary, the characteristic times and probabilities were calculated and the relaxation times were calculated as solutions to linear systems of a few (usually up to five) variables. Kinetic Monte Carlo[60] was used to eliminate the intermediates from the rate matrices and predict observable transition counts. Using the sequence of visited states enabled us to exclude intermediates and count overall transitions between the observable states. For 3D clusters, the rates were calculated for lower friction constant values and extrapolated to the experimental value.

TABLE I. The number of experimentally observed transitions between structures in 92266 s and corresponding rate constants in s^{-1}.[3] Where the forward and backward number of transitions do not match, the average has been taken.

Transition	T $\leftrightarrow$ C	T $\leftrightarrow$ P	C $\leftrightarrow$ P
Transitions Observed	52	63	139
rate/s^{-1}	5.64×10^{-4}	6.83×10^{-4}	1.51×10^{-3}
Relative rates	1	1.2	2.2

III. RESULTS AND DISCUSSION

A. Two-Dimensional Clusters

1. Experimental Results

The two-dimensional experimental results are reported in Ref. 3. Four stable structures are observed, referred to as the triangle (T), the chevron (C) and the parallelogram (P), which has two enantiomers P1 and P2, all of which have nine nearest-neighbour contacts (or "bonds"). The parallelogram is chiral and cannot be converted to its enantiomer without breaking a contact. However, the enantiomers are treated together in the experiment. Since the interactions of the particles are short-ranged, all the minima have very similar, although not quite identical, potential energies. Such sets of structures are referred to as quasi-degenerate.[5] Considering the energy and symmetry only (i.e. disregarding rotational and vibrational contributions), the ratio of minima (T : C : P1 : P2) should be 2:6:3:3 regardless of temperature. The fact that this ratio is experimentally observed (after combination of the two parallelograms) suggests that rotational and vibrational contributions to entropy are negligible. The rates of conversion between structures were estimated by observing a cluster for 25.6 hours and simply counting the transitions. These data are reproduced in table I.

2. Characterisation of the structures

A system of six Morse discs constrained to a sufficiently large box has only four minima, corresponding to the experimental T, C and P. These minima are structures 1-4 in Fig. 1. Since the parallelogram is chiral and cannot be converted into its optical isomer without breaking a contact, we will distinguish isomers and consider them as separate states. There are 11 transition states with 8 contacts, shown in Fig. 1.

3. Estimation of the Experimental Well Depth

An indication of the appropriate well depth for comparison with experiment can be obtained from the populations of structures with 9 and 8 contacts. The ratio of equilibrium populations for separate 8-contact states is more difficult to calculate. In addition to the symmetry number and
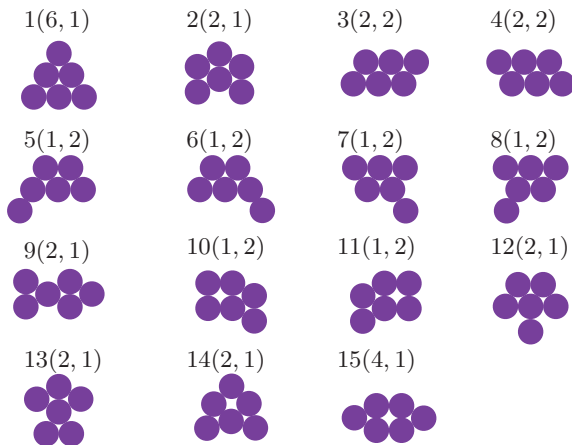
FIG. 1. Structures. The first number is the structure label used in the text and tables below. The numbers in parentheses are the symmetry numbers and the number of enantiomers, respectively.

TABLE II. Equilibrium populations (in %) of various structures for the Morse$_6^{2D}$ cluster at five selected reciprocal temperatures β (first column). The next three columns contain the equilibrium populations of the triangle, chevron and one enantiomer of the parallelogram, respectively. Equilibrium populations for all structures with 8 contacts (structures 5-15) are summed in column 5, for structures 16-36 summed in column 6, and the last column contains the sum of populations for all structures with fewer than 7 contacts.

β	1	2	3	8 B	7 B	< 7 B
3.0	0.1	0.2	0.1	1.0	1.8	96.8
6.0	7.6	25.5	11.9	27.8	10.7	4.5
7.0	11.0	36.3	16.6	15.9	3.0	0.5
8.0	10.8	41.5	19.6	7.9	0.5	0.0
9.0	13.8	43.5	19.8	3.1	0.1	0.0

chirality, it is strongly influenced by the freedom of those particles (or sub-structures) connected to the rest of the cluster by a single contact. In some cases this freedom is caused by the possibility of a diamond-square-diamond[61] or similar transition. Equilibrium populations of the 37 states for 13 different inverse temperatures between $\beta = 3$ and $\beta = 9$ were calculated by parallel tempering Monte Carlo (PTMC) simulations. The accuracy of the results can be estimated by a comparison of values for enantiomers (table II).

4. Transition State Theory

The dimensionless rate constants for the transitions were calculated using TST and are shown in table III for three different well depths. The forward and backward rate constants were multiplied by the fraction of the population in that minimum at equilibrium as determined by the free energy, to give the transition rates. Free energies were cal-

TABLE III.

Structure	T	C	P
% population	14.5	44.1	41.4
$\beta\epsilon_0$	T $\leftrightarrow$ C	T $\leftrightarrow$ P	C $\leftrightarrow$ P
Natural Units τ_0^{-1}			
6.0	2.01×10^{-3}	4.23×10^{-3}	6.00×10^{-3}
7.0	7.37×10^{-4}	1.55×10^{-3}	2.20×10^{-3}
8.0	2.69×10^{-4}	5.66×10^{-4}	8.03×10^{-4}
Experimental units s^{-1}			
6.0	7.01	14.8	20.9
7.0	2.78	5.84	8.29
8.0	1.08	2.28	3.24
Relative rates	1	2.1	3.0

culated using the harmonic superposition approach.[62]

Table III shows that, as expected due to the neglect of diffusion along the path, the TST rates are large overestimates. The rates are in the correct order, although the ratios between them do not agree quantitatively with experiment. The approximate correction factor required to adjust the TST rates to the experimental rates, assuming a well depth of $6k_BT$, is around 1.6×10^{-4}.

5. 2D Discrete Relaxation Path Sampling

Besides four 9-contact states, we divided the configuration space into 33 additional states defined by their unique topology and chirality. Out of these 33 states, 11 have 8 contacts, 21 have 7 contacts (one of these is actually a cluster of five particles and a separated particle, see App. A). Since the 8-contact states have the shape of a long narrow channel, each was divided into smaller cells to enhance sampling. Structures with fewer than 7 contacts are not of experimental interest, so were lumped into a single state. States defined in this way are compact and can be directly observed in experiments. Transitions can occur only between topological neighbours by breaking or establishing a contact. The dynamical properties were calculated using DRPS.[28] Since the 11 8-contact structures were divided into 90 cells, the rate matrix obtained from DRPS described transitions between 115 cells.

Pairwise relaxation times calculated using DRPS converge rapidly compared to the simulation time for this system. Doubling the computational resources for DRPS results in changes of around 5%. The average length of a simulated trajectory increases linearly with the friction constant. As the friction increases, the trajectories become longer but less probable and very short trajectories (corresponding to recrossing a boundary) are more commonly sampled. The convergence is faster at lower friction, when more trajectories can be simulated for a given computational cost.

The equilibrium populations obtained from DRPS agree with the PTMC results. We found that the equilibrium populations converge more slowly than the relaxation times with computational cost using the DRPS protocol for this system. We found similarly slow convergence with boxed

TABLE IV. The predicted number of transitions observed per 26 hours calculated at various β. The experimental values can be found in table I.

$\beta\epsilon_0$	T $\leftrightarrow$ C	T $\leftrightarrow$ P	C $\leftrightarrow$ P
6.0	2500	2200	6100
7.0	1000	1000	3100
Relative rate ($\beta\epsilon_0 = 7$)	1	1	3.1

molecular dynamics[30] and hyperdynamics.[29] The reason for this difference is probably the bimodal distribution of return times, characteristic of systems with large friction. The final rate matrix was constructed from the relaxation times obtained from DRPS and equilibrium populations from PTMC.
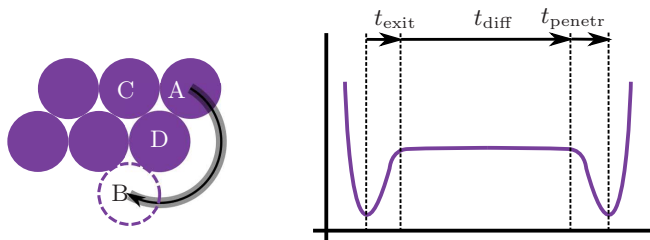
FIG. 2. LEFT: The most likely transition mechanism from P to C at low temperature is via structure 6. The top right disc (A) moves along the indicated path to the final position (B) marked by a dashed circle. One contact with a neighbouring disc (C) is broken. To avoid breaking another contact (with disc D), the centre of disc A is constrained to a narrow channel denoted by the grey curve. RIGHT: If the friction constant is large, the diffusion time for moving along the channel (t_{diff}) is greater than the characteristic time for breaking the contact between discs A and C (t_{exit}). When the disc reaches structure 2, the time to relax to the equilibrium C structure (t_{penetr}) is small.

The resulting rate matrix was then used in kinetic Monte Carlo (KMC) simulations, to reproduce the experimental results. After 10^5 KMC transitions, the number of transitions between the triangle, chevron and parallelograms expected in 25.6 hours was calculated. The calculated values for $\beta\epsilon_0 = 7$ reasonably agree with the experimental ones (table IV).

The simulations of thermodynamics suggest that the system can be viewed as a collection of highly populated minima with low-populated diffusive barriers between them. Hence, flux-based approaches with correction factors[25,26] can give correct results. However, trajectories terminated at the boundaries of 9-contact states are so long that TPS would be computationally expensive. Enhanced sampling methods based on space cutting are applicable as the high friction causes rapid loss of memory. Among other enhanced sampling methods, milestoning[31] and transition interface sampling[63] (and partial path transition interface sampling[64] in particular) could be efficient. The relaxation approach leads to the exact result if the Markovian assumption holds for all cells. This requirement would be satisfied if the 8-contact states were divided into thousands of small

cells. The DRPS rate for a process in which a system diffuses through a number of large cells will always be lower than the true rate. DRPS provides a robust and reasonably accurate estimate for the rates.

B. Three-Dimensional clusters

1. Experimental Results

The experimental results for the 3D system are described in Ref. 1. Two quasi-degenerate stable states with 12 nearest neighbour contacts were observed: a polytetrahedron (point group C_{2v}) and an octahedron (point group O_h). The population ratio is approximately 1:20, explained principally by the relative number of permutational isomers,[6] with smaller contributions from the rotational and vibrational entropies. A precise interconversion rate is not reported, but the authors state they "observed transitions between the two states on time scales of minutes", suggesting a rate constant of around $10^{-2}\,\text{s}^{-1}$ to $10^{-3}\,\text{s}^{-1}$.

2. Characterisation of the structures

Two minima were found for the system of six-particle Morse clusters in 3D space, corresponding to the experimentally observed polytetrahedron (structure A) and the octahedron (structure B). At $\beta\epsilon_0 = 6$, the predicted population ratio is 21.6:1. The minima are discussed in greater detail in Ref. 6. Five transition states with 11 contacts were also located. Four of these transition states lie on paths between permutational isomers of structure A; only one lies on a path interconverting structure A and structure B. These structures are shown in Fig. 3.
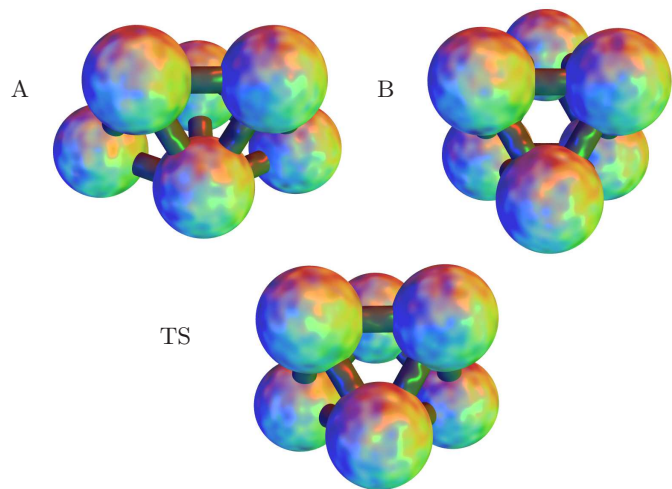

FIG. 3. A: the polytetrahedron. TS: the transition state between the two structures with C_{2v} symmetry. B: the octahedron. The bonds indicate nearest-neighbour contacts.

3. Estimation of the Experimental Well Depth

To estimate the well depth of the experimental attraction, Monte Carlo simulations of the three-dimensional system were performed at temperatures of $\beta\epsilon_0 = 4, 5, 6$ in a container with a diameter of $d_c = 4\sigma_0$. Energy histograms of the structures sampled in these simulations are plotted in Fig. 4. The histograms consistently show that a high proportion of clusters are dissociated at temperatures $\beta\epsilon_0 < 5$. The clusters are barely stable at $\beta\epsilon_0 = 5$ and relatively stable at $\beta\epsilon_0 = 6$. From the experimental value of the ratio of dissociated clusters to compact ones, it is possible to estimate the temperature with a confidence of two significant figures.
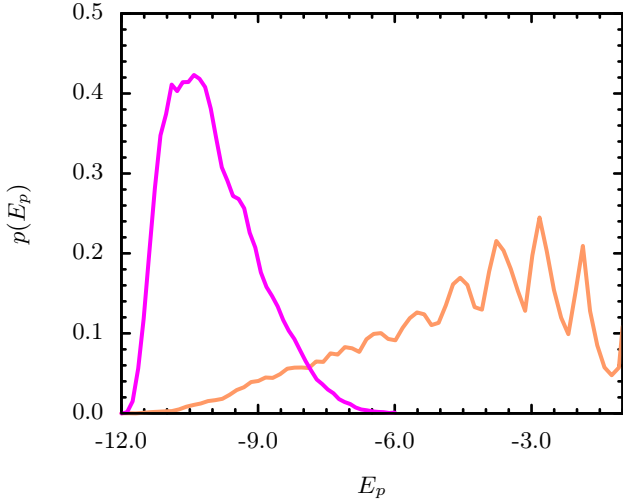

FIG. 4. Energy histograms at reciprocal temperature $\beta\epsilon_0^{3D} = 4$ (orange) and $\beta\epsilon_0^{3D} = 6$ (purple) obtained with Monte Carlo simulations. The container diameter was $r_c = 4\sigma_0^{3D}$.

The instability of the cluster at $\beta\epsilon_0^{3D} = 4$ is explained by the following back-of-the-envelope calculation. Breaking one contact will free a particle from a well of width $r_{\text{width}} \approx 0.05\sigma_0^{3D}$ (determined by the range of the interaction), so that it can slide along a surface through a distance $r_{\text{slide}} \approx \sigma_0^{3D}$. One contact breakage is associated with an entropic gain of $\Delta S_1 \approx k_B \log(r_{\text{slide}}/r_{\text{width}}) \approx 3k_B$. Since there are 12 contacts that can be broken (adding $k_B \log 12$ to the entropic gain $\sim 2.5k_B$), the energetic gain of one contact has to be at least $5.5k_BT$ for the 12-contact cluster to be at least as stable as the 11-contact one. We therefore suggest that a value of $\epsilon_0^{3D} \geq 6k_BT$ is appropriate.

4. Transition State Theory and the Geometrical Approach

The dimensionless TST rate for interconversion of structures A and B at $\beta\epsilon_0^{3D} = 6$ is $\tau_0^{3D} = 1.76 \times 10^{-3}$ s, giving a rate of $12.1 \, \text{s}^{-1}$ in experimental units. Again, this value is too high due to the neglect of spatial diffusion. A correction factor of the order of 10^{-3} to 10^{-4} is required for agreement with the experimental value.

The geometrical approach of Holmes-Cerfon et al.[24] produced a promising agreement with experimental values for the 2D clusters.[3] The TST rates have been calculated for the 6, 7 and 8 particle 3D clusters to compare with the results for the geometrical approach given in Ref. 24. Only those transitions that are not between permutational isomers of the same structure are included. For both approaches, the dimensionless values are used. Fig. 5 shows a clear correlation between the two methods. The fitted correction factor is 0.0043.
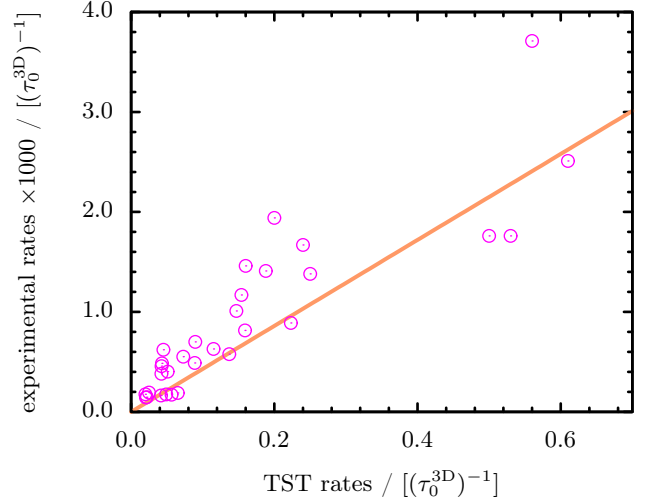

FIG. 5. Comparison of the geometrical rate constants and the TST rate constants.

5. 3D Discrete Relaxation Path Sampling

The configuration space was partitioned into two cells corresponding to structures A and B by Voronoi construction. A fingerprinting metric was used to distinguish structures rather than the root mean square distance, to avoid using heuristic permutational-rotational alignment of the clusters.[65] To calculate the overlap of a given structure X with structure A, all 15 mutual distances between atoms in X were calculated. Values of the fingerprinting function f_A (Fig. 6) at the three shortest distances longer than $r_{\text{min}} = 1.2\sigma_0^{3D}$ were summed to estimate the overlap. The same procedure was repeated with the fingerprinting function f_B to calculate the overlap with structure B. A structure was assigned to the state with greater fingerprint overlap. This metric is somewhat similar to that used by Perry et al.[3] for 2D clusters.

The DRPS method[28] was used to calculate the rate constants $k_{A\rightarrow B}$ and $k_{B\rightarrow A}$.

1. 1000 structures were obtained by Monte Carlo simulations constrained to each cell. The structures were sampled after 5000 normally distributed steps with mean displacement of $0.004\sigma_0^{3D}$ in every dimension.
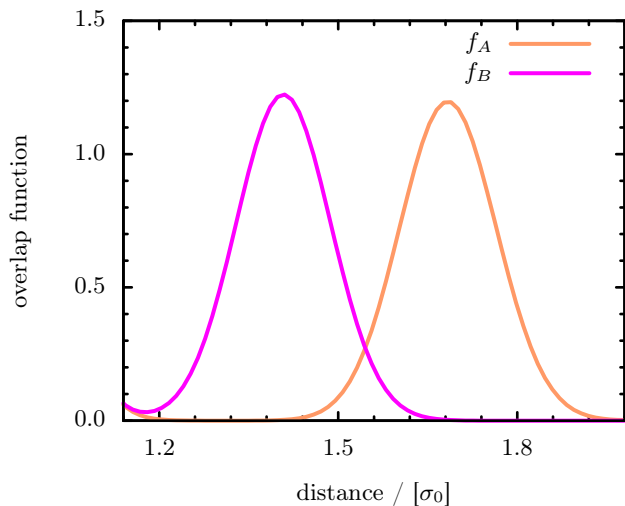
FIG. 6. Fingerprinting overlap functions for structure A (orange) and structure B (purple). The non-bonding distances (3 longest distances for a compact cluster) are larger for the polytetrahedron (A) than for the octahedron (B).

FIG. 7. Relaxation times calculated for low friction (triangles) scale linearly, so we extrapolate them to high friction (square).

2. One trajectory was propagated to both sides from each of these structures until it reached the boundary.

3. The system of linear equations derived in Ref. 28 was solved to calculate the relaxation time.

To increase the sampling efficiency, the cluster was constrained to a spherical container with radius $r_{\max} = 3\sigma_0^{3D}$. The centre of this container was identified with the centre of mass of the cluster at each step.

The calculations were performed for $\gamma\tau_0^{3D}/\mu_0^{3D} = 5, 10, 20$ and 40. Calculations for higher values of γ were computationally expensive (more than an hour on one CPU), as the computer time scales linearly with the characteristic time of the event. To increase the speed of the simulation, further partitioning of space would be required. However, this additional effort is not really necessary. The high value of the friction constant suggests that the system is in the high-damping regime, where the rate constant is directly proportional to the diffusion coefficient $k \propto 1/\gamma$.[22] A quantitative criterion for the applicability suggested in a previous report was the ratio of the DRPS (correct) relaxation time to the relaxation time calculated from the first exit times.[66–68] The ratio for any value of γ was above 0.93, suggesting that even at $\gamma = 20\mu_0^{3D}/\tau_0^{3D}$ the system is in the high-damping regime. In this case, we can calculate the rate constant for large γ by extrapolating the line $\tau_{\rm rxn} = C/\gamma$. The expected relaxation time is about 0.4 s, so the expected waiting time between two successive transitions is 10 s in state A and 0.4 s in state B. The results for this reciprocal temperature agree well with experiments.
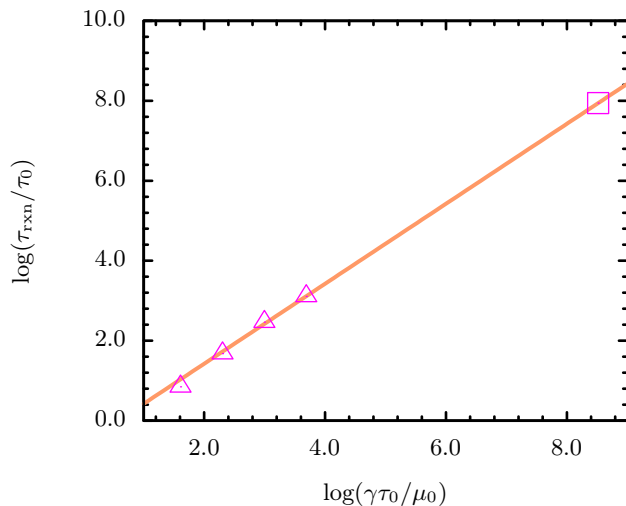
IV. CONCLUSIONS

Equilibrium populations of clusters observed experimentally are consistent with simulations when the interaction energy between the particles is just below $\epsilon_0^{2D} \approx 7k_BT$ and $\epsilon_0^{3D} \approx 6k_BT$. We suggest that values between $6k_BT$ and $7k_BT$ may be more appropriate than $4k_BT$.[1,5]

TST proved to be inadequate to describe the transitions between clusters, since the theory does not include spatial diffusion along the path after contact breaking. Even though the potential energy changes negligibly along the long narrow channel the particle has to traverse during the transition, random forces from the solvent and the SDS micelles (2D clusters) or PNIPAM spheres (3D system) can reverse the particle direction towards the original state. A correction factor of the order 10^{-4} appears to be appropriate for the transitions considered. When compared to the geometric theory, there is then a reasonable correlation between the geometric rate and the TST rate.

The results estimated by DRPS are in promising agreement with experiment. One reason for the remaining differences might be errors in estimation of the friction constant. The apparent hydrodynamic friction for the two-dimensional cluster may be increased by the SDS film used to attach the spheres to the cover. The agreement would probably be better if a more accurate (experimentally determined) value of the interaction energy was used.

can be accessed on `http://github.com/borislavujo/` `publications/tree/master/morse6.`

---

[1] G. Meng, N. Arkus, M. P. Brenner, and V. N. Manoharan, Science **327**, 560 (2010).

[2] R. W. Perry, G. Meng, T. G. Dimiduk, J. Fung, and V. N. Manoharan, Faraday Discuss. **159**, 211 (2012).

[3] R. W. Perry, M. C. Holmes-Cerfon, M. P. Brenner, and V. N. Manoharan, Phys. Rev. Lett. **114**, 228301 (2015).

[4] P. M. Morse, Phys. Rev. **34**, 57 (1929).

[5] F. Calvo, J. P. K. Doye, and D. J. Wales, Nanoscale **4**, 1085 (2012).

[6] D. J. Wales, ChemPhysChem **11**, 2491 (2010).

[7] A. Malins, S. R. Williams, J. Eggers, H. Tanaka, and C. P. Royall, J. Phys. Condens. Matter **21**, 425103 (2009).

[8] J. Taffs, A. Malins, S. R. Williams, and C. P. Royall, J. Phys. Condens. Matter **22**, 104119 (2010).

[9] J. W. R. Morgan and D. J. Wales, Nanoscale **6**, 10717 (2014).

[10] E. Bianchi, R. Blaak, and C. Likos, Phys. Chem. Chem. Phys. **13**, 6397 (2011).

[11] J. W. Merrill, S. K. Sainis, and E. R. Dufresne, Phys. Rev. Lett. **103**, 138301 (2009).

[12] M. Polanyi, Z. Phys. **2**, 90 (1920).

[13] L. Farkas, Z. Physik. Chem. **125**, 236 (1927).

[14] H. Pelzer and E. Wigner, Z. Phys. Chem. Abt. B **15**, 445 (1932).

[15] H. Eyring, Chem. Rev. **17**, 65 (1935).

[16] M. G. Evans and M. Polanyi, T. Faraday. Soc. **31**, 875 (1935).

[17] H. Eyring, J. Chem. Phys. **3**, 107 (1935).

[18] M. G. Evans and M. Polanyi, T. Faraday. Soc. **33**, 448 (1937).

[19] W. F. K. Wynne-Jones and H. Eyring, J. Chem. Phys. **3**, 492 (1935).

[20] E. Wigner, Trans. Faraday Soc. **34**, 0029 (1938).

[21] E. Wigner, J. Chem. Phys. **7**, 646 (1939).

[22] H. A. Kramers, Physica **7**, 284 (1940).

[23] P. Hanggi, P. Talkner, and M. Borkovec, Rev. Mod. Phys. **62**, 251 (1990).

[24] M. Holmes-Cerfon, S. J. Gortler, and M. P. Brenner, Proc. Natl. Acad. Sci. U.S.A. **110**, E5–E14 (2013).

[25] D. Chandler, J. Chem. Phys. **68**, 2959 (1978).

[26] C. Dellago, P. G. Bolhuis, F. S. Csajka, and D. Chandler, J. Chem. Phys. **108**, 1964 (1998).

[27] C. Dellago and P. G. Bolhuis, *Transition Path Sampling and Other Advanced Simulation Techniques for Rare Events*, Adv. Polym. Sci. Advances in Polymer Science, **221**, 167 (2009).

[28] B. Fačkovec, E. Vanden-Eijnden, and D. J. Wales, J. Chem. Phys. **143**, 044119 (2015).

[29] A. F. Voter, J. Chem. Phys. **106**, 4665 (1997).

[30] D. R. Glowacki, E. Paci, and D. V. Shalashilin, J. Phys. Chem. B **113**, 16603 (2009).

[31] A. K. Faradjian and R. Elber, J. Chem. Phys. **120**, 10880 (2004).

[32] V. S. Pande, K. Beauchamp, and G. R. Bowman, Methods **52**, 99 (2010).

[33] G. R. Bowman, V. S. Pande, and F. Noé, *An Introduction to Markov State Models and Their Application to Long Timescale Molecular Simulation* (Springer, 2014).

[34] G. Elfving, Acta Soc. Sci. Fennicae **8**, 1 (1937).

[35] B. V. Derjaguin and L. D. Landau, Acta. Phys. Chim. USSR **14**, 633 (1941).

[36] E. J. W. Verwey and J. T. G. Overbeek, *Theory of the Stability of Lyophobic Colloids* (Elsevier, Amsterdam, 1948).

[37] R. Verberg, I. M. de Schepper, and E. G. D. Cohen, Phys. Rev. E **55**, 3143 (1997).

[38] Z. Li and H. A. Scheraga, Proc. Natl. Acad. Sci. U.S.A. **84**, 6611 (1987).

[39] Z. Li and H. A. Scheraga, J. Mol. Struc-Theochem **179**, 333 (1988).

[40] D. J. Wales and J. P. K. Doye, J. Phys. Chem. A **101**, 5111 (1997).

[41] D. J. Wales and H. A. Scheraga, Science **285**, 1368 (1999).

[42] D. J. Wales, "GMIN: A program for basin-hopping global optimisation, basin-sampling, and parallel tempering," http://www-wales.ch.cam.ac.uk/software.html (1999).

[43] S. A. Trygubenko and D. J. Wales, J. Chem. Phys. **120**, 2082 (2004).

[44] J. M. Carr, S. A. Trygubenko, and D. J. Wales, J. Chem. Phys. **122**, 234903 (2005).

[45] G. Henkelman and H. Jónsson, J. Chem. Phys. **111**, 7010 (1999).

[46] G. Henkelman, B. P. Uberuaga, and H. Jónsson, J. Chem. Phys. **113**, 9901 (2000).

[47] G. Henkelman and H. Jónsson, J. Chem. Phys. **113**, 9978 (2000).

[48] J. N. Murrell and K. J. Laidler, T. Faraday. Soc. **64**, 371 (1968).

[49] L. J. Munro and D. J. Wales, Phys. Rev. B: Condens. Matter Mater. Phys. **59**, 3969 (1999).

[50] D. J. Wales, "OPTIM: A program for optimising geometries and calculating pathways," http://www-wales.ch.cam.ac.uk/software.html (1999).

[51] D. J. Wales, "PATHSAMPLE: A program for generating connected stationary point databases and extracting global kinetics," http://www-wales.ch.cam.ac.uk/software.html (1999).

[52] D. J. Wales, Mol. Phys. **100**, 3285 (2002).

[53] D. J. Wales, Mol. Phys. **102**, 891 (2004).

[54] S. A. Trygubenko and D. J. Wales, J. Chem. Phys. **124**, 234110 (2006).

[55] S. A. Trygubenko and D. J. Wales, Mol. Phys. **104**, 1497 (2006).

[56] D. J. Wales, Int. Rev. Phys. Chem. **25**, 237 (2006).

[57] D. J. Wales, J. Chem. Phys. **130**, 204111 (2009).

[58] N. Metropolis, A. W. Rosenbluth, M. N. Rosenbluth, A. H. Teller, and E. Teller, J. Chem. Phys. **21**, 1087 (1953).

[59] D. A. Sivak, J. D. Chodera, and G. E. Crooks, The Journal of Physical Chemistry B **arxiv.org** (2013).

[60] D. T. Gillespie, J. Comput. Phys. **22**, 403 (1976).

[61] W. N. Lipscomb, Science **153**, pp. 373 (1966).

[62] D. J. Wales, *Energy Landscapes* (Cambridge University Press, Cambridge, 2003).

[63] T. S. van Erp, D. Moroni, and P. G. Bolhuis, J. Chem. Phys. **118**, 7762 (2003).

[64] D. Moroni, P. G. Bolhuis, and T. S. van Erp, J. Chem. Phys. **120**, 4055 (2004).

[65] D. J. Wales and J. M. Carr, J. Chem. Theory Comput. **8**, 5020 (2012).

[66] S. Northrup and J. Hynes, J. Chem. Phys. **69**, 5246 (1978).

[67] K. Schulten, Z. Schulten, and A. Szabó, J. Chem. Phys. **74**, 4426 (1981).

[68] D. Bicout and A. Szabo, J. Chem. Phys. **106**, 10292 (1997).
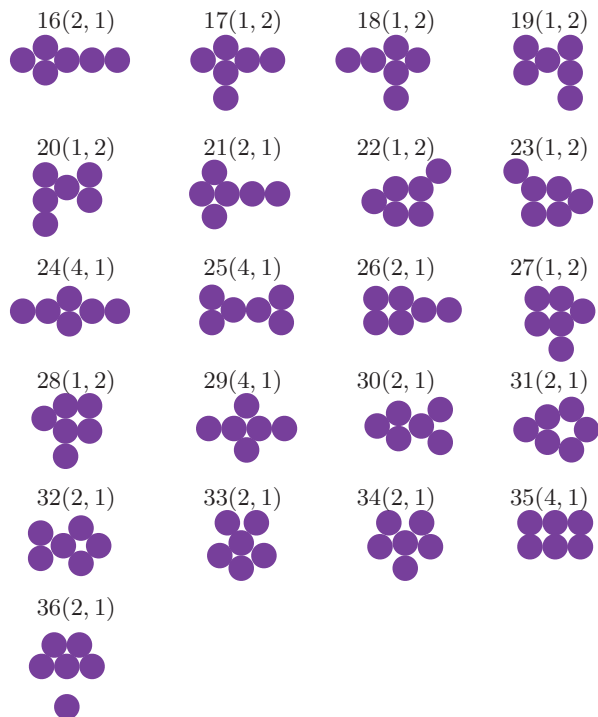
Appendix A: Additional structures

FIG. 8. Structures with fewer than 8 contacts. The first number is the structure label used in the main text and tables; the numbers in the parentheses are the symmetry numbers and the number of enantiomers, respectively.